MAGNETIC RESONANCE IN CHEMISTRY, VOL. 34, S87–S96 (1996)

NMR and Paramagnetic Ion Substitution Locates a Modified-Nucleoside Dependent Metal Binding Site in DNA: Molecular Dynamics, Surface Charge and H_2O Ordering

Paul F. Agris,* John W. Stuart and Richard Guenther
Department of Biochemistry, North Carolina State University, Raleigh, North Carolina 27695-7622, USA

Mufeed M. Basti
Department of Chemistry, North Carolina A & T University, Greensboro, North Carolina 27412, USA

The NMR-derived structure, dynamics and metal binding of a unique 17-residue DNA stem and loop hairpin were determined. The hairpin binds one Mg^{2+} ion and is a biologically active DNA analogue of the yeast $tRNA^{Phe}$ anticodon domain only when two naturally occurring modified nucleosides, $d(m^5C)$ and $d(m^1G)$, are site selectively incorporated. The modified nucleosides aided in signal assignments in lieu of isotope labeling. Signal assignments were accomplished for 80% of the exchangeable and non-exchangeable protons. Titration of the DNA with Mn^{2+}, monitored by ^1H NMR spectroscopy, indicated that the Mg^{2+} binding site is located in the loop of the hairpin at the bottom of the stem. The binding of Mg^{2+} contributed to loop stability. Loop dynamics were evidenced by line broadness on the methyl signal of $d(m^1G)$ and were compared with that of an identical tDNA stem and loop hairpin that lacked the $d(m^1G)$ modification but contained $d(m^5U)$. TDNA hairpin dynamics are discussed in the light of the Mg^{2+} binding constants for the two $tDNA^{Phe}$. A highly refined, Mg^{2+}-bound structure of the $tDNA^{Phe}_{AC}$ is presented along with computer-simulated effects of Mg^{2+} on the tDNA's net surface charge and surface of H_2O.

KEY WORDS NMR; ^1H NMR; DNA solution conformation; metal binding site; paramagnetic substitution; tRNA anticodon analogue; modified nucleosides

INTRODUCTION

More than 100 post-transcriptional modifications contribute to the chemistry, structure and function of nucleic acids.[1,2] The physico-chemical contributions of modified nucleosides have been compared with the chemical contributions made by amino acid side-chains to proteins, i.e. hydrophobic or hydrophilic (polar or charged).[2] One of ten postulated results of nucleic acid modification is the production of specific metal ion binding sites.[2] Mg^{2+} binding to nucleic acids has a vital role in both structure and function and the literature is replete with physical and biochemical data correlating modified nucleosides to RNA's binding of Mg^{2+}.[3–11] Electrostatic interactions of local concentrations of counterions with nucleic acids can affect conformational dynamics and intermolecular interactions.[12] Conformational changes subsequent to Mg^{2+} binding are important for biological activity.[2] Although the role of Mg^{2+} as a counterion to the RNA phosphodiester backbone had been recognized,[13] only with the determination of the yeast $tRNA^{Phe}$ structure from x-ray crystallography were Mg^{2+} ions found tightly bound within a nucleic acid.[14] However, at that time the relationship of modified nucleosides to high-affinity Mg^{2+} ion binding and the resulting RNA conformation was neither obvious nor experimentally approachable.

Native $tRNA^{Phe}$ has 4–5 high-affinity Mg^{2+} binding sites[15] (Fig. 1) and approximately 50 weaker sites.[16] At least one of the high-affinity Mg^{2+} binding sites is in the $tRNA^{Phe}$ anticodon domain, $tRNA^{Phe}_{AC}$ (Fig. 1). Native $tRNA^{Phe}_{AC}$, a heptadecamer with five modified nucleosides (Fig. 1), binds the ribosome with the same kinetics as the entire tRNA molecule.[17] Analysis of nuclear Overhauser effects (NOEs) of a 15mer native anticodon domain by 1D difference spectroscopy resulted in assignment of base and H1′ protons.[18] A structural model, developed from NMR data, compared favorably with the crystal structure. Using CD and NMR spectroscopy of ribonucleoside heptadecamers, we confirmed the existence of a modification-dependent, high-affinity Mg^{2+} binding site in the anticodon domain of yeast $tRNA^{Phe}$.[18] Mg^{2+} binding resulted in a conformational transition of the anticodon.[19] Our study showed that high-affinity Mg^{2+} binding by the $tRNA^{Phe}_{AC}$ was dependent upon methylation of cytidine at position 40 in the $tRNA^{Phe}$ anticodon stem (m^5C_{40}). This was the first documented example of a single modification facilitating RNA coordination of Mg^{2+}.

To test our understanding of the m^5C_{40}-dependent Mg^{2+} binding and to assess the possible role of the ribose 2′-OH in metal coordination, DNA analogues

* Author to whom correspondence should be addressed.

CCC 0749–1581/96/SI0087–10

Received 10 June 1996
Accepted (revised) 6 September 1996

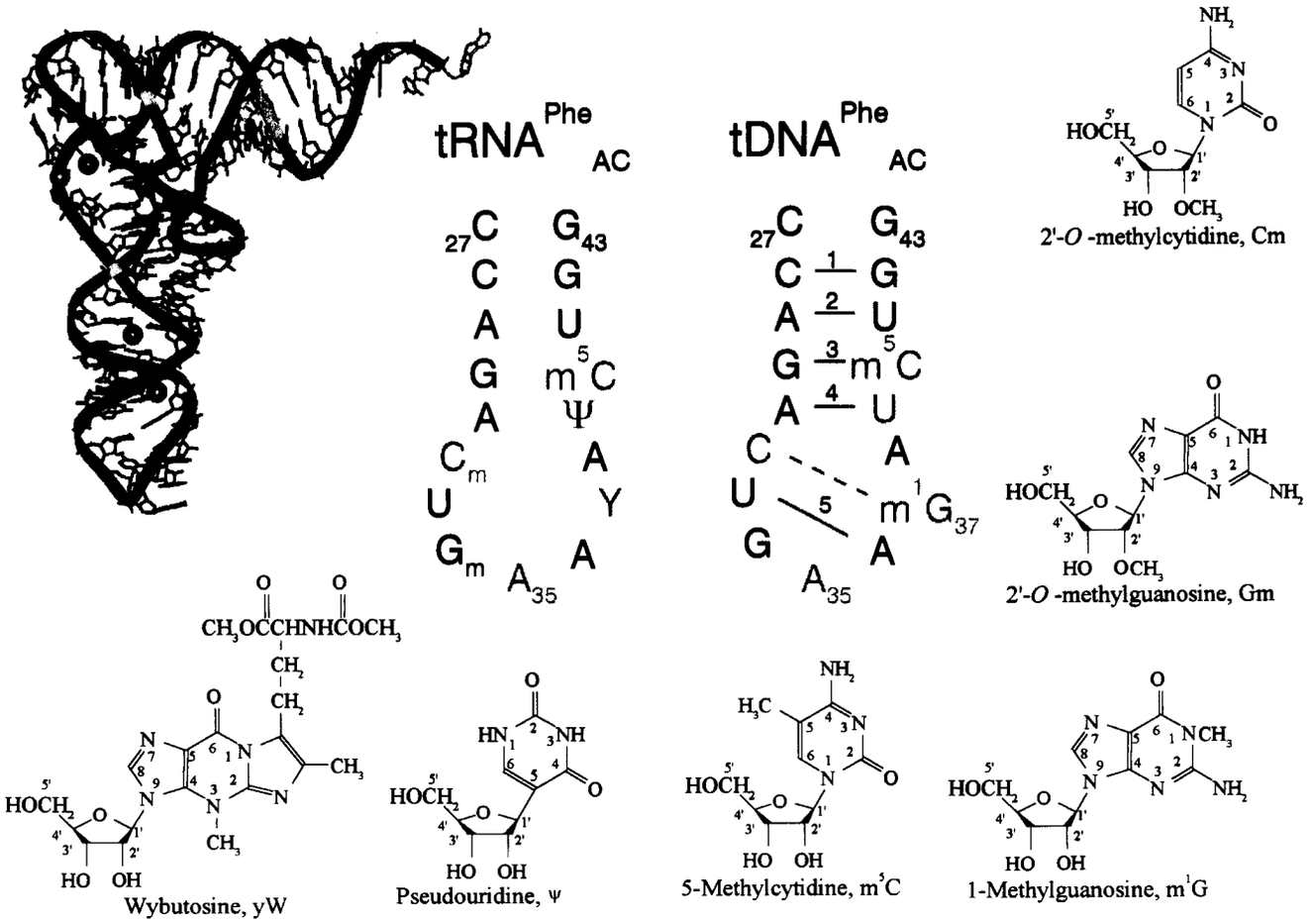

Figure 1. Left: three-dimensional structure of yeast $tRNA^{Phe}$ determined by x-ray crystallography.[14] Mg^{2+} ions are represented by gray spheres. Right: schematic representations of the primary sequence and secondary structures of the anticodon region of native $tRNA^{Phe}$ with five modified nucleosides, Cm_{32}, Gm_{34}, yW (Y_{37}), ψ_{39} and m^5C_{40}, and $tDNA^{Phe}_{AC}$ with two modified deoxynucleosides, $d(m^5C_{40})$ and $d(m^1G_{37})$. Numbered base pairs correspond to imino signals in Fig. 6. Bottom and side: chemical structures of the five modified nucleosides in $tRNA^{Phe}_{AC}$ and m^1G.

($tDNA^{Phe}_{AC}$) with modified deoxynucleosides and dU substituting for dT (Fig. 1) were synthesized and tested for Mg^{2+} coordination. $tDNA^{Phe}_{AC}$ exhibited a $d(m^5C_{40})$-dependent, high-affinity Mg^{2+} binding that produced a conformational transition.[20,21] With the addition of a second modification, $d(m^1G_{37})$, in the loop of the hairpin designated $tDNA^{Phe}_{AC}$–$d(m^1G_{37}; m^5C_{40})$, the molecule bound the ribosome and inhibited native $tRNA^{Phe}$ from binding. The structure of the biologically active $tDNA^{Phe}_{AC}$–$d(m^1G_{37}; m^5C_{40})$ was determined from NMR-derived distance and torsion angle restraints;[22] however, the location of Mg^{2+} was not determined. Here, we present the NMR-determined localization of the Mg^{2+}, a refined structure of the $tDNA^{Phe}_{AC}$ and effects of Mg^{2+} on the molecules net surface charge and surface H_2O.

EXPERIMENTAL

Synthesis of DNA

The native anticodon domain of yeast $tRNA^{Phe}$ contains five naturally occurring post-transcriptional modifications: 2′-*O*-methylcytidine at position 32 (Cm_{32}), 2′-*O*-methylguanosine-34 (Gm_{34}), wybutosine-37 (yW_{37}, Y_{37}), pseudouridine-39 (ψ_{39}) and 5-methylcytidine-40 (m^5C_{40}) (Fig. 1). The oligodeoxynucleotides used in this study were heptadecamers with the base sequence analogous to the tRNA's anticodon domain (Fig. 1). For this study, $d(m^1G_{37})$ was substituted for the more chemically labile yW_{37}. All oligodeoxynucleotides were synthesized using standard DNA phosphoramidite chemistry on an Applied Biosystems Model 394 automated synthesizer.[23] The modified and protected phosphoramidite $d(m^1G)$ was prepared as described previously.[24] The protected $d(m^5C)$, dU and all standard deoxynucleoside phosphoramidites were purchased from Glen Research. Oligonucleotides were purified by ion-exchange high-performance liquid chromatography.[24] Successful incorporation of the modified nucleosides was verified by a quantitative nucleoside composition analysis.[25] Concentrations were determined spectrophotometrically at 260 nm using an extinction coefficient of 1.60×10^6 l mol^{-1} cm^{-1}.[26] The DNA analogue of the unmodified anticodon domain was designated $tDNA^{Phe}_{AC}$. Modified analogues are identified by naming the modified nucleosides that they contain, following the residue numbering system of

native yeast $tRNA^{Phe}$; i.e. $tDNA^{Phe}_{AC}$-d(m^1G_{37} ; m^5C_{40}) (Fig. 1).

Determination of tDNA thermal stability prior to NMR

UV absorbance at 260 nm was monitored over the temperature range 5–85 °C using a Gilford spectrophotometer with Response II software. For each oligonucleotide, measurements were made over the range 0.5–25 μM. Both 1 and 10 mm cuvettes were used to maintain a proper optical response. Samples were prepared in the same buffer to be used for NMR analyses, i.e. 10 mM sodium phosphate buffer (pH 7). Samples were thermally denatured, renatured and the process repeated one more time to determine the reversibility of the transition. In all cases less than 1 °C difference in T_m was recorded between melting and annealing. The T_m was independent of tDNA concentration, indicating a unimolecular transition. Calculations of the thermodynamic parameters ΔH, ΔS and ΔG were made assuming a two-state unimolecular model following published methods.[27] Values presented are the average of six thermal denaturations, two experiments at three different concentrations. Denaturations were internally normalized to percentage of absorbance at 90 °C for each experiment and the melting curve analyzed with a linear regression.

NMR measurements

$tDNA^{Phe}_{AC}$-d(m^1G_{37} ; m^5C_{40}) was dissolved in 10 mM sodium phosphate buffer (pH 7) in H_2O or D_2O. The final concentration of the NMR sample was 1.3 mM. $MgCl_2$ was added to the sample to a final Mg^{2+} concentration of 5 mM. No monovalent salt was added to the sample. NMR experiments were conducted as described.[22] Briefly, four types of two-dimensional homonuclear correlation spectroscopic experiments were performed: TOCSY,[28] 2QFCOSY,[29] jump-and-return NOESY[30] and NOESY.[31] Generally, 1024 × 256 complex points were acquired for 2D experiments (GE Omega 500 MHz spectrometer) using States *et al.*'s method to acquire phase-sensitive data[32] and transformed by the appropriate window functions and baseline corrections with FELIX version 2.1 (Biosym Technologies, San Diego, CA, USA) to yield 1024 × 1024 complex matrices. NOESY experiments in H_2O were acquired on a Bruker 500 MHz spectrometer (TPPI method for phase cycling[33]). Unless stated otherwise, NOESY spectra were processed with a combination of a sine-bell window function shifted by 30° and a line broadening of 3 Hz. Proton-decoupled ^{31}P NMR spectra were acquired at 202 MHz; ^{31}P chemical shifts were referenced to the trimethyl phosphate signal set at 0 ppm. tDNA was titrated with Mn^{2+} by incremental (20 μM) additions of a 10 mM $MnCl_2$ solution. The broadness of the exchangeable proton signals was observed to indicate the position of the Mn^{2+} binding.

Restrained molecular dynamics

The $tDNA^{Phe}_{AC}$-d(m^1G_{37} ; m^5C_{40}) model structure was derived from NMR data as described previously.[22] Briefly, initial distance constraints were generated with FELIX version 2.1 using a two-spin approximation and a bounds range of ±20%. NOESY cross-peak volume build-ups of the non-exchangeable protons were used to generate a full relaxation matrix (Iterative Relaxation Matrix Analogue, IRMA, Biosym Technologies). Restrained molecular dynamics (rMD) and energy minimization (rEM) calculations included 235 distance and dihedral angle constraints. Simulated rMD calculations, ten iterations of 10 ps at 500 K (Discover module-AMBER force field, Biosym Technologies), searched conformational space for structures consistent with NMR constraints. The five-step rMD/rEM calculations included three energy minimization steps. The resultant structure was used as the initial structure for the next step of IRMA calculations. IRMA–rMD/rEM iterative calculations were concluded when the correlative R factor between the constraint-generated and theoretical structures attained the value 0.014.

Computational methods for ion placement

To initiate computation of a single Mg^{2+} ion's binding to $tDNA^{Phe}_{AC}$-d(m^1G_{37} ; m^5C_{40}), an Mg^{2+} was placed at the base of the stem in the loop of the tDNA solution structure model.[22] No other NMR-derived distance restraints were applied to the model. In placing the Mg^{2+}, overlap of van der Waals radii was avoided. The Mg^{2+} location was determined from ^1H NMR experiments in which line broadenings were observed during Mn^{2+} titration of the tDNA. All calculations were performed with Discover3 (Biosym/MSI) using the AMBER force field[34] on a Silicon Graphics IRIS Indigo workstation. The following conditions were used unless noted otherwise. Force field parametizations for m^1G and m^5C have been published.[22] The base pairs in the stem were kept planar at the standard distance using torsional and distance restraints, respectively. To make the system electrically neutral, 14 Na^+ counterions were placed in the plane made by the phosphates, except for residues dU_{33} and dA_{38}, since they were most perturbed by Mg^{2+} when minimized *in vacuo*. The solvated system was initially minimized for 500 steps using steepest descent with an 8 Å residue-based nonbond cut-off, constant dielectric function, all-atom force field and periodic boundary conditions with cell size 35 × 50 × 35 Å. A 100 ps molecular dynamic (MD) simulation was performed with constant pressure using velocity scaling to maintain a constant temperature of 300 K. A 1.0 fs time step was used with RATTLE to fix the bonds of TIP3P waters. A subset of stable water molecules was found by searching for molecules with low translational deviation over the last 50 ps of the MD.

Electrostatic potentials, $\phi(r)$, were calculated using DelPhi[35] with charges from the AMBER force field. There was no significant difference in the tDNA's electrostatic potential whether calculated by DelPhi with the salt entirely absent or at a concentration of 0.145 M. Therefore, an exterior dielectric constant of 80 with 0.145 M salt (near saline) was assumed with an interior dielectric constant of 2 for the tDNA molecule. Surface

$\phi(r)$s of $tDNA^{Phe}_{AC}$ were visualized using InsightII (Biosym/MSI).

RESULTS AND DISCUSSION

Mg^{2+} binding and $tDNA^{Phe}$ thermal stability studies prior to NMR

A deoxynucleoside sequence, $tDNA^{Phe}_{AC}$–d(m^1G_{37}; m^5C_{40}), was designed and synthesized to emulate as closely as possible the sequence of the heptadecamer anticodon stem and loop domain of yeast $tRNA^{Phe}$ (Fig. 1). The $tDNA^{Phe}_{AC}$ sequence included two modified nucleosides, d(m^5C_{40}) and d(m^1G_{37}). The d(m^5C_{40}) provided an Mg^{2+} binding site that stabilized the $tDNA^{Phe}$ structure[20,21] and d(m^1G_{37}), by negating the formation of a canonical $dC_{32}\cdot dG_{37}$ base pair, maintained an open loop important for the analogue to bind the ribosome and inhibit tRNA from binding.[17] Another $tDNA^{Phe}_{AC}$ was chemically synthesized with only one of the two modifications, d(m^5C_{40}). $tDNA^{Phe}_{AC}$–d(m^5C_{40}), with a dT_{33} instead of a dU_{33}, had a loop closed by two canonical base pairs[20,21] and was biologically inactive.[17] The location and coordinating ligands of the Mg^{2+} in $tDNA^{Phe}_{AC}$–d(m^1G_{37}; m^5C_{40}) had not been determined and compared with that of native $tRNA^{Phe}$. In addition, the effects of Mg^{2+} on structure, stability and surface electrostatics had not been determined.

In preparation for NMR experiments, the stability of $tDNA^{Phe}_{AC}$–d(m^1G_{37}; m^5C_{40}) structure with and without Mg^{2+} was assessed by UV-monitored thermal denaturations (Fig. 2). Mg^{2+} sharpened the denaturation profile and increased T_m from 42.8 ± 0.5 to 47.0 ± 0.7 °C (Fig. 2). A magnesium binding constant for $tDNA^{Phe}_{AC}$–d(m^1G_{37}; m^5C_{40}) was determined from the

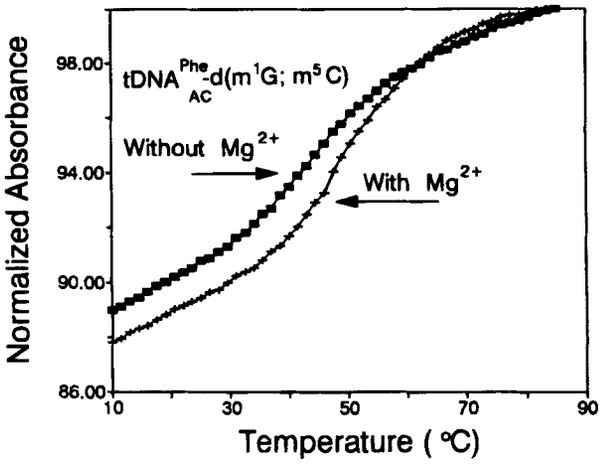

Figure 2. Thermal denaturations of $tDNA^{Phe}_{AC}$–d(m^1G_{37}; m^5C_{40}) in the presence and absence of 10 mM Mg^{2+}.

T_m data. T_m was sensitive to Mg^{2+} in a concentration-dependent manner. T_m was measured, at two $tDNA^{Phe}_{AC}$ concentrations, over a range of Mg^{2+} concentrations. Assuming a stoichiometry of 1:1,[20,21] the K_d was calculated at each DNA and magnesium concentration and then averaged. The K_d by this method was $7.8 \pm 3.4 \times 10^{-4}$ l mol^{-1}. At an Mg^{2+} concentration of 5 mM, all $tDNA^{Phe}_{AC}$–d(m^1G_{37}; m^5C_{40}) would be expected to be complexed with Mg^{2+} in NMR studies.

NMR signal assignments

Assignments of 132 of 167 exchangeable[22] and non-exchangeable protons (Table 1) were achieved by a series of one- and two-dimensional NMR experiments. Imino base-paired protons were assigned from 1D 'jump and return' NOE difference spectra.[22] Exchange-

Table 1. Non-exchangeable ^1H NMR chemical shifts of $tDNA^{Phe}_{AC}$–d(m^1G_{37}; m^5C_{40})

	Chemical shift (ppm)							
Residue	H1′	H2′	H2″	H3′	H4′	H5′, H5″	H6/H8	H5/H2
dC_{27}	5.89	2.07	2.45	4.62	4.06	3.71	7.71	5.85
dC_{28}	5.30	2.04	2.30	4.81	—	4.08/3.97	7.57	5.65
dA_{29}	5.86	2.73	2.84	5.03	4.36	4.16/3.83	8.21	7.53
dG_{30}	5.52	2.49	2.64	5.01	—	4.36/4.16	7.69	—
dA_{31}	6.21	2.47	2.55	4.79	—	4.40/4.12	8.09	—
dC_{32}	5.99	1.94	2.32	4.70	4.60	4.16/3.93	7.52	5.63
dU_{33}	5.87	2.34	2.43	4.75	—	3.69/3.51	7.53	5.44
dG_{34}	5.38	—	—	—	—	—	—	—
dA_{35}	5.69	—	2.44	4.87	—	—	8.03	—
dA_{36}	5.87	2.33	2.39	4.74	—	4.38/4.16	7.99	—
d(m^1G_{37})	6.19	2.13	2.49	4.82	—	4.27	7.69	1.66[a]
dA_{38}	6.08	2.69	2.69	—	—	4.21	8.18	7.40
dU_{39}	5.98	2.07	2.55	4.83	—	4.26	7.60	5.33
d(m^5C_{40})	5.96	2.24	2.38	4.85	—	4.17/4.10	7.44	1.73[a]
dU_{41}	5.63	2.03	2.35	4.74	—	4.15	7.57	5.48
dG_{42}	5.68	2.69	2.69	4.98	4.35	4.11	7.86	—
dG_{43}	5.68	2.48	2.71	5.17	4.48	4.41/4.30	7.78	—

[a] Methyls of d(m^5C_{40}) and d(m^1G_{37}).

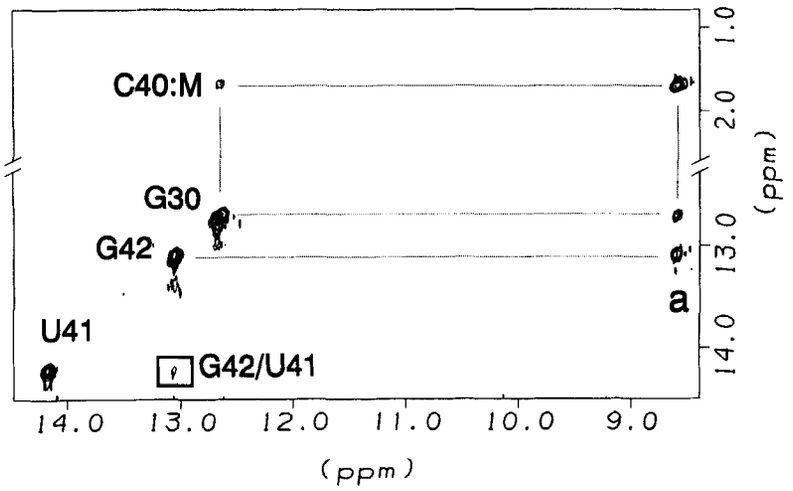

Figure 3. Signal assignments in the imino proton section of the 'jump and return' NOESY spectrum of $tDNA_{AC}^{Phe}$–d(m^1G_{37} ; m^5C_{40}) are aided by the presence of a base modification. Signals in the diagonal of the spectrum correspond to three of the imino base paired protons: U41, $dA_{29}\cdot dU_{41}$; G42, $dC_{28}\cdot dG_{42}$; G30, $dG_{30}\cdot d(m^5C)_{40}$. The methyl of $d(m^5C)_{40}$ is coupled to the imino base paired proton of $dG_{30}\cdot d(m^5C)_{40}$, C40:M. Correlations are noted for two of the exchangeable imino protons G42/U41, $dC_{28}\cdot dG_{42}$ and $dA_{29}\cdot dU_{41}$, and between the $dC_{28}\cdot dG_{42}$ imino base pair and the G amino, a. The spectrum was taken with the tDNA in H_2O at 10 °C and with a 400 ms mixing time. The spectrum was processed with a combination of a 40°-shifted sine-squared function and 5 Hz line broadening.

able proton assignments were confirmed with data from 2D, 'jump and return' NOESY spectra, such as the $dC_{28}\cdot dG_{42}$ to $dA_{29}\cdot dU_{41}$ coupling shown in Fig. 3. Modified nucleosides with their unique spin systems can be used as assignment probes. We used the methyl signals of $d(m^5C_{40})$ and $d(m^1G_{37})$ to assign signals originating from the corresponding and the neighboring residues. The number of NOEs that the two methyls displayed facilitated their use as assignment probes in a manner similar to the use of isotopic labeling. The position of $d(m^1G_{37})$ in the loop of the $tDNA_{AC}^{Phe}$–d(m^1G_{37} ; m^5C_{40}) hairpin facilitated the assignment of the broader NMR lines emanating from the more dynamic nucleosides of the loop. The methyl of $d(m^5C_{40})$ aided in the imino base-paired signal assignments of the stem. The $dG_{30}\cdot d(m^5C_{40})$ imino base-paired proton was coupled to the methyl of $d(m^5C_{40})$ (Fig. 3). Assignments of non-exchangeable proton signals were achieved through DQF-COSY and NOESY spectra. For instance, the scalar connections between the 1′ and 2′ and 2″ protons were resolved in the DQF-COSY spectrum (Fig. 4. Every nucleoside exhibited an H1′–H2′ coupling, but some stem residues also exhibited 1′–2″ couplings. Assignments of pyrimidine residue aromatic protons were accomplished through the H6–H5 scalar and dipolar couplings in the DQF-COSY and NOESY spectra, respectively (data not shown).

Proton signals originating from the well structured stem, where bases were stacked, were shaper than the signals originating from the loop. In the loop bases, for the most part, were not stacked and chemical and structural dynamics were evident. Sequence-specific assignments were attained by studying the section of the NOESY spectra, at four different mixing times, that exhibited dipolar coupling of the purine H2 and H8 and pyrimidine H5 and H6 to the H1′, H2′, H2″ and the methyls of $d(m^5C_{40})$ and $d(m^1G_{37})$. Sequence specific connectivities were aided by the trivial assignments of the two methyls (Fig. 5). The H2″ of the *n* residue had a dipolar coupling to the aromatic H6 or H8 of the $n + 1$ residue.[36] NMR spectra of $tDNA_{AC}^{Phe}$–d(m^1G_{37} ; m^5C_{40}) indicated that the stacking was improved on the 3′-side of the dG_{30}–$d(m^5C_{40})$ base pair in the stem and on the 3′-side of the loop in the vicinity of m^1G_{37}. In the loop, the normal sequential H2″–H8 dipolar coupling was stronger around $d(m^1G_{37})$ than in any other section of the loop. Thus, in both stem and loop, the simple base modification of methylation induced significant structural changes in the tDNA. A methyl group-restricted base motion and structural change has also been reported for methylation of dA at N6 in a TpA site of a double helical DNA.[37]

All $tDNA_{AC}^{Phe}$–d(m^1G_{37} ; m^5C_{40}) residues displayed the intra-residue H2′–H6 or H8 NOEs that indicate an *anti* conformation around the glycosidic bond. Every deoxyribose adopted the 2′-*endo* conformation; the H1′–H2″ coupling was 1–2 Hz. In the H1′–H2′, H2″ region of the DQF-COSY spectrum H1′–H2′ peaks dominated H1′–H2″ peaks for most residues of the tDNA. The narrow range of 0.8 ppm of the ^{31}P chemical shifts and the -3.5 ppm chemical shift also indicated that both stem and loop residues adopted the 2′-*endo* conformation.[22] One ^{31}P resonance whose integration corresponded to a single phosphorous was shifted about 2 ppm downfield and was attributed to the phosphodiester bond at the dU_{33} 'U' turn in the structure.[22] Residues 27–31 and 39–43 in the stem of hairpin exhibited both H1′–H2′ and H1′–H2″ cross peaks, indicating that the sugar moieties in these residues were in slow exchange on the NMR time-scale between the 2′-*endo* conformation and some other pucker.[38] The imino base pair signals of the stem were not affected by presaturation of the H_2O resonance, thereby confirming stem structural stability on the time-scale of base pair disruption. The slow exchange process could have been part of an overall 'breathing' of the stem helical structure or due to the chemical exchange experienced by the whole molecule when Mg^{2+} is bound to the loop. Since the last base pair of the stem, $dA_{31}\cdot dU_{39}$, was the only stem imino proton affected

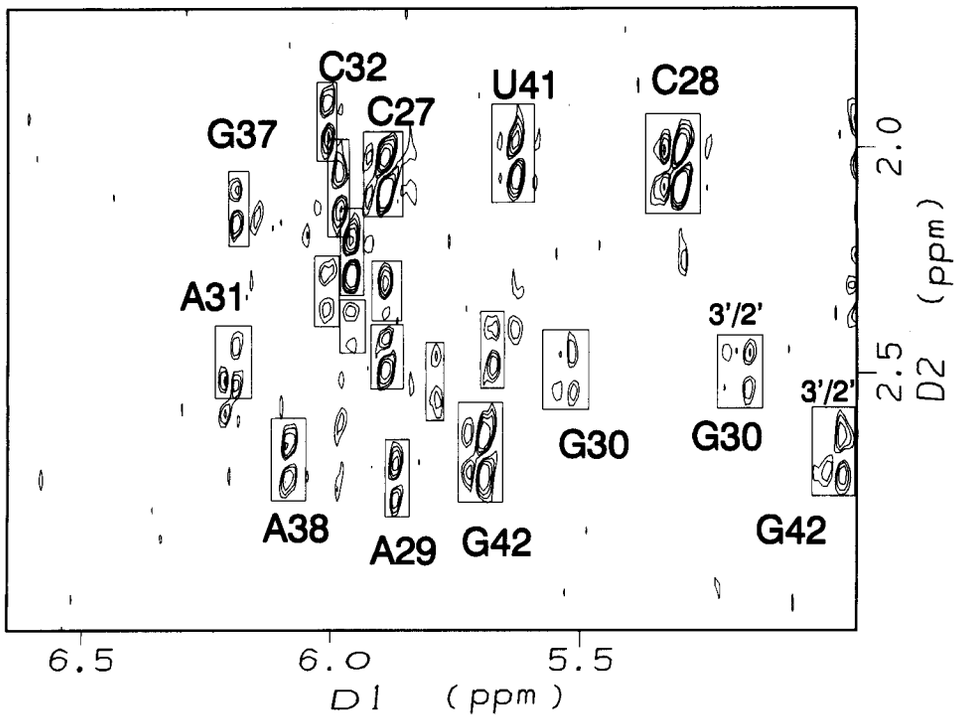

Figure 4. DQF-COSY spectrum of $tDNA_{AC}^{Ph}$•. The H1′–H2′ and H1′–H2″ scalar couplings are observed in a section of the DQF-COSY spectrum. Some of the couplings are attributed to their respective nucleosides. In addition, two H3′–H2′ couplings are assigned. The spectrum was taken with the sample in buffered D_2O and 10 °C. The spectrum was processed with a combination of 30°-shifted sine-squared and 0.5 Hz exponential line broadening window functions.

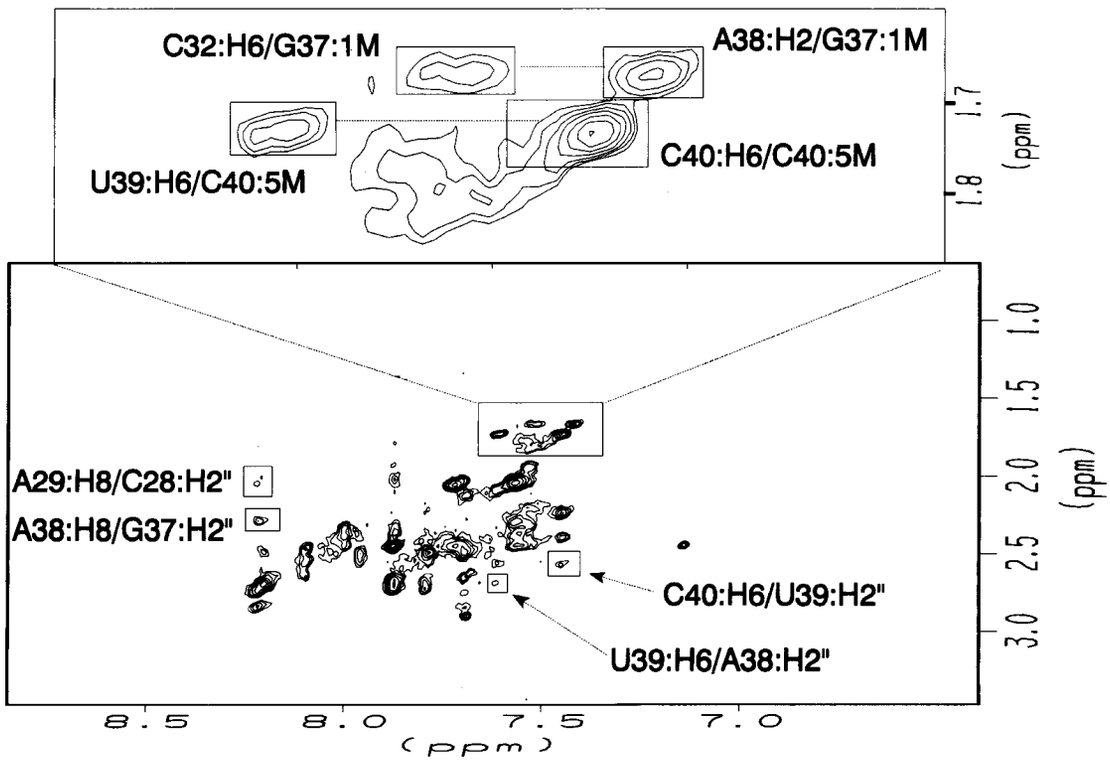

Figure 5. Methyls aid in sequential assignments. A section of a NOESY spectrum is shown in which H6 and H2 to methyl NOEs and the sequential H8 or H6 to H2′ and H2″ NOEs are evident. A small part of the spectrum is enlarged to detail NOEs involving the methyls of $d(m^1G_{37})$ and $d(m^5C_{40})$. Besides NOEs to sequentially adjacent nucleosides, the NOE from the methyl of $d(m^1G_{37})$ across the loop to the H6 of dC_{32} is of particular interest and importance to the structure. The spectrum was taken at 10 °C with a 200 ms mixing time. The spectrum was processed with a combination of 10°-shifted sine-squared and 3 Hz exponential line broadening window functions.

by Mg^{2+}, structure and dynamics of the stem were considered independent of Mg^{2+}.

Structure refinement and chemical dynamics of the $tDNA^{Phe}_{AC}$–d(m^1G_{37} ; m^5C_{40}) loop

Further refinement of the previously published $tDNA^{Phe}_{AC}$–d(m^1G_{37} ; m^5C_{40}) structure[22] was attained by comparing the experimental and theoretically calculated NOEs and by use of gradient terms to direct the structure refinement process (Biosym Technologies). The molecule's rational correlation time of 4 ± 0.2 ns had been determined previously.[22]

The comparison of experimental and theoretically calculated NOEs included a penalty function (with a restraint force of 50 kcal mol^{-1} $Å^{-2}$) which reflected the discrepancy between the theoretical and experimental NOE volumes. The penalty function and its gradient with respect to atomic Cartesian coordinates were incorporated into the overall restraint energy. The aim of the process was to improve the fit between the experimental and the theoretical NOE volumes, which in turn led to the refinement of the three dimensional structure. However, the d(m^1G_{37}-dependent open loop structure of the molecule was dynamic. The $tDNA^{Phe}_{AC}$–d(m^1G_{37} ; m^5C_{40}) loop's chemical dynamics with one intra-loop base pair, $dU_{33} \cdot dA_{36}$, was compared with that of $tDNA^{Phe}_{AC}$–d(m^5C_{40}) with a loop constrained by two canonical base pairs, $dC_{32} \cdot dG_{37}$ and $dT_{33} \cdot dA_{36}$. The methyl signals of d(m^1G_{37}) in the loop of $tDNA^{Phe}_{AC}$–d(m^1G_{37} ; m^5C_{40}) and that of dT_{33} in the loop of $tDNA^{Phe}_{AC}$–d(m^5C_{40}) were compared at different temperatures. The methyl of dT_{33} in $tDNA^{Phe}_{AC}$–d(m^5C_{40}) exhibited slow dynamics, two resolved signals at low temperature, whereas the methyl signal of d(m^1G_{37}) in the loop of $tDNA^{Phe}_{AC}$–d(m^1G_{37} ; m^5C_{40}) exhibited fast dynamics, a single but broad resonance for a methyl. The faster loop dynamic of $tDNA^{Phe}_{AC}$–d(m^1G_{37} ; m^5C_{40}) was evidenced by the disappearance of resonances for the $dA_{31} \cdot dU_{39}$ base pair at the bottom of the stem and the $dU_{33} \cdot dA_{36}$ intra-loop base pair upon presaturation of the H_2O signal. The $dC_{28} \cdot dG_{42}$, $dA_{29} \cdot dU_{41}$ and $dG_{30} \cdot d(m^5C_{40})$ base pair signals were not affected by presaturation of the H_2O (data not shown). Thus, the appearance of the d(m^1G_{37}) methyl resonance, the absence of any H1′–H2″ DQF-COSY cross peaks from the loop's residues and the disappearance of the loop's base pair signals with H_2O presaturation were all indications that the $tDNA^{Phe}_{AC}$–d(m^1G_{37} ; m^5C_{40}) loop's dynamics are fast on the NMR time-scale.

Evidence of chemical exchange kinetics of $tDNA^{Phe}_{AC}$ has been published.[20,21] Some of this evidence was obtained with NMR, but most with circular dichroism spectropolarimetry. The NMR data were qualitative and indicated that the chemical exchange was in the loop. However, the CD data were quantitative and produced the reported Mg^{2+} binding constant. The affinity of $tDNA^{Phe}_{AC}$–d(m^1G_{37} ; m^5C_{40}) for Mg^{2+} was lower by a factor of 10 than that of $tDNA^{Phe}_{AC}$–d(m^5C_{40}) with two intra-loop base pairs. We propose that this lower Mg^{2+} binding constant was one reason for the loop's dynamics; the loop was adopting Mg^{2+}-bound and Mg^{2+}-unbound structures. An Mg^{2+}-induced change in the anticodon of $tRNA^{Phe}$ has been detected by yW fluorescence and other methods.[7] Mg^{2+} binding constants are at least 100-fold higher for native *vs.* unmodified *E. coli* $tRNA^{Val}$.[8] In the absence of Mg^{2+}, fully modified *E. coli* and yeast $tRNA^{Phe}$ existed in two or more conformations in slow exchange that could be detected in NMR spectra by observation of ^{13}C enriched methyls.[3,9–11] This fluorescence study of a 15-mer native yeast $tRNA^{Phe}$ anticodon domain demonstrated the presence of at least two Mg^{2+} binding sites of different affinities and an RNA conformational change correlated to Mg^{2+} complexation.[39]

Paramagnetic ion substitution of Mg^{2+}

Locating the Mg^{2+} in the tDNA molecule would help explain the stability provided by metal ion binding and, perhaps, explain how the presence of d(m^5C_{40}) introduced the single Mg^{2+} binding site. In order to locate correctly the position of Mg^{2+} in the $tDNA^{Phe}_{AC}$–d(m^1G_{37} ; m^5C_{40}), we experimented with various metal ion substitutions that could be advantageous to NMR and/or EPR studies.[40] The conformation of $tDNA^{Phe}_{AC}$–d(m^5C_{37}), detected by circular dichroism spectropolarimetry, in the presence of 1 mM Cd^{2+}, Co^{2+}, Cr^{2+}, Cu^{2+}, Ni^{2+}, Pb^{2+}, VO^{2+} or Zn^{2+}, differed significantly from that of the biologically active structure resulting from interaction with Mg^{2+}, Mn^{2+} or Ca^{2+}. Nanomolar concentrations of the transition metals were sufficient to denature the $tDNA^{Phe}_{AC}$–d(m^5C) structure without catalyzing cleavage of the oligonucleotide. Since Mn^{2+} is a paramagnetic metal ion, upon binding to a molecule selective line broadening of ^1H NMR signals occurred and was indicative of the location of the metal ligand. Mn^{2+} has been used to observe ion binding to a structural alteration induced by the whole rG·rU base pair in a tRNA acceptor arm.[41] Mn^{2+} titration of a molecule the size of the tDNA (*ca.* 5500 Da) that produced well resolved NMR spectra and whose assignments were almost complete was advantageous in locating the Mg^{2+} binding site. The CD spectrum of $tDNA^{Phe}_{AC}$–d(m^1G_{37} ; m^5C_{40}) in Mn^{2+} was identical with that of the biologically active $tDNA^{Phe}_{AC}$–d(m^1G_{37} ; m^5C_{40}) in Mg^{2+} (data not shown). Therefore, to identify the Mg^{2+} binding site, the Mg^{2+}-containing $tDNA^{Phe}_{AC}$–d(m^1G_{37} ; m^5C_{40}) sample in H_2O was titrated with a 10 mM solution of $MnCl_2$ until the $[Mn^{2+}]/[tDNA]$ ratio was 1:6.5. NMR spectra were acquired after each addition of Mn^{2+} (Fig. 6). The exchangeable-proton and methyl signals were the most informative resonances. Spectra indicated clearly that the peak corresponding to the $dA_{31} \cdot dU_{39}$ base pair at the bottom of the loop was most affected by the earliest of Mn^{2+} additions. Interestingly, the resonance corresponding to the $dG_{30} \cdot d(m^5C_{40})$ base pair was not affected by the Mn^{2+} addition, yet the single-site Mg^{2+} binding is dependent on the presence of d(m^5C_{40}). The methyl resonance of d(m^1G_{37}), but not the methyl of d(m^5C_{40}), was affected by the Mn^{2+}. Other resonances were affected by higher concentrations of Mn^{2+} with some relationship to the distance of the protons from

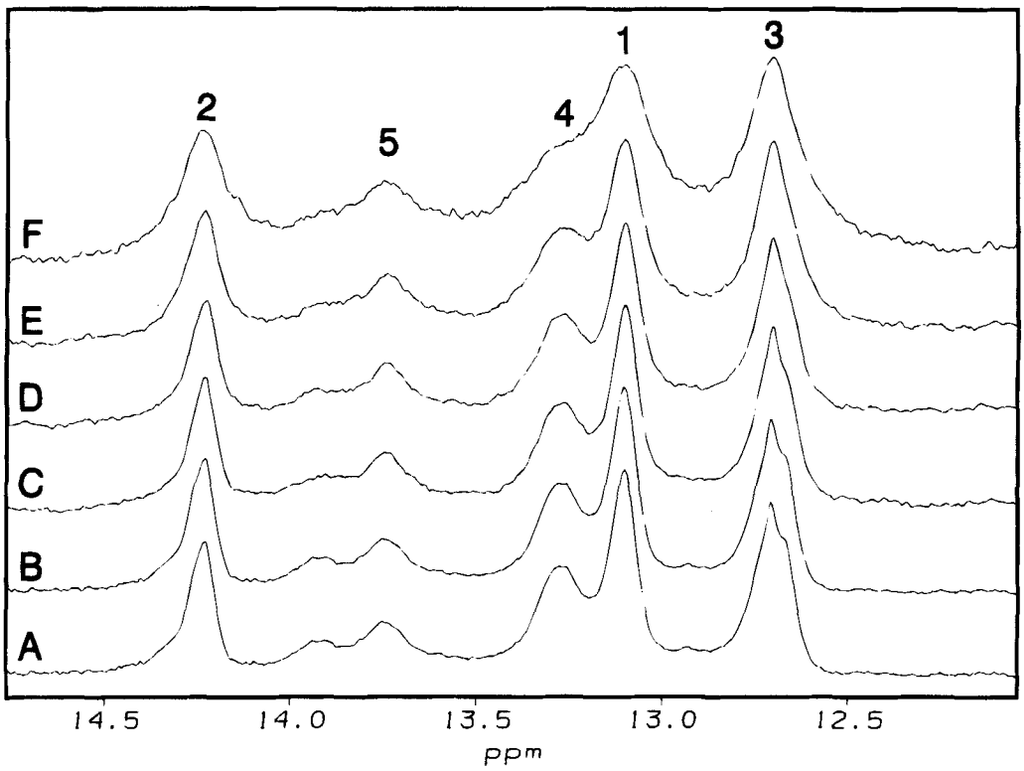

Figure 6. Changes in the imino proton signals of $tDNA^{Phe}_{AC}$–d(m^1G_{37} ; m^5C_{40}) when titrated with Mn^{2+}. Spectra of $tDNA^{Phe}$ in H_2O were taken with 5 mM Mg^{2+}, but in the absence of Mn^{2+} (A) or with increasing concentrations of Mn^{2+}: (B) 0.02; (C) 0.04; (D) 0.08; (E) 0.12 and (F) 0.20 mM. Signal assignments 1–5 correspond to base pairs $dC_{28} \cdot dG_{42}$, $dA_{29} \cdot dU_{41}$, $dG_{30} \cdot d(m^5C_{40})$, $dA_{31} \cdot dU_{39}$ and $dU_{33} \cdot dA_{36}$, respectively.

the loop binding site, as exemplified by resonances 3 and 5 as compared with 1 and 2 in Fig. 6.

Placement and coordination of the Mg^{2+} in the $tDNA^{Phe}_{AC}$–d(m^1G_{37} ; m^5C_{40}) loop

Results of Mn^{2+} paramagnetic broadening of ^1H NMR signals placed the Mg^{2+} binding site in the $tDNA^{Phe}_{AC}$–d(m^1G_{37} ; m^5C_{40}) loop near the last base pair of the stem, $dA_{31} \cdot dU_{39}$ and the methyl of d(m^1G_{37}). Examination of the electrostatic surface of the NMR solution structure revealed a large space where the bottom of the stem bends into the loop region, a location large enough to accommodate binding of a hydrated Mg^{2+}. Since the previous structure did not contain Mg^{2+}, the $tDNA^{Phe}_{AC}$ was modeled using MD to determine if the presence of Mg^{2+} would induce any global conformational changes. With the Mg^{2+} placed approximately in the area of highest potential for binding, the $tDNA^{Phe}_{AC}$ was solvated with 1707 water molecules and neutralized with 14 Na^+ ions, filling the cell volume. The structure was minimized and subjected to 100 ps of MD simulation. the 100 ps time-scale seemed sufficient to sample conformational space since the structure converged rather quickly and the overall magnitude of deviation was small (Fig. 7). For the entire simulation, the Mg^{2+} ion remained situated between the bases of dC_{32} and dA_{38}. The Mg^{2+} was coordinated by the carbonyl oxygen of dC_{32}, the N1 of A_{38} and four water molecules (Plate 1, left). In contrast, the one Mg^{2+} in the anticodon of the yeast $tRNA^{Phe}$ x-ray crystallographic structure (Fig. 1) was coordinated to five H_2Os (which were in turn H-bonded to nucleosides) and to the 5′-phosphate of yW (Y_{37}) (Plate 1, right). Because the binding site determination was largely driven by electrostatic calculations on solutions structures, an analogous calculation in solution with hydrated Mg^{2+} was conducted with the $tRNA^{Phe}$ crystal restraints. The resulting structure had the Mg^{2+} localized to a position identical to that of the Mg^{2+} in the crystal. Thus, placement of Mg^{2+} in the $tDNA^{Phe}_{AC}$ analogue in solution was close to the stem, whereas its location in the $tRNA^{Phe}$ crystal structure was close to the anticodon. $tRNA^{Phe}_{AC}$ had a higher affinity for Mg^{2+}

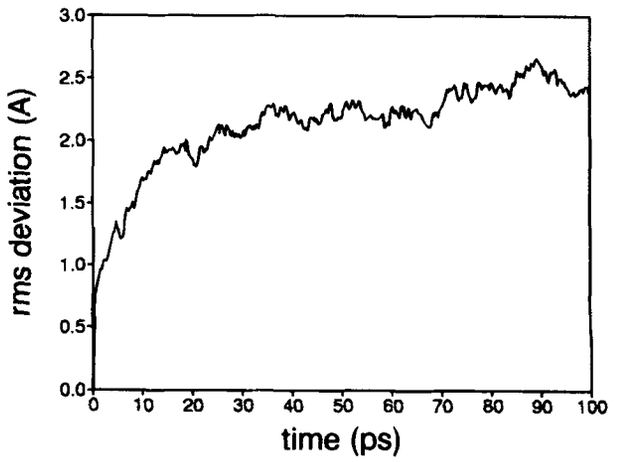

Figure 7. The rms deviation of heavy atoms of $tDNA^{Phe}_{AC}$ with bound Mg^{2+} from NMR derived structure *vs.* simulation time.

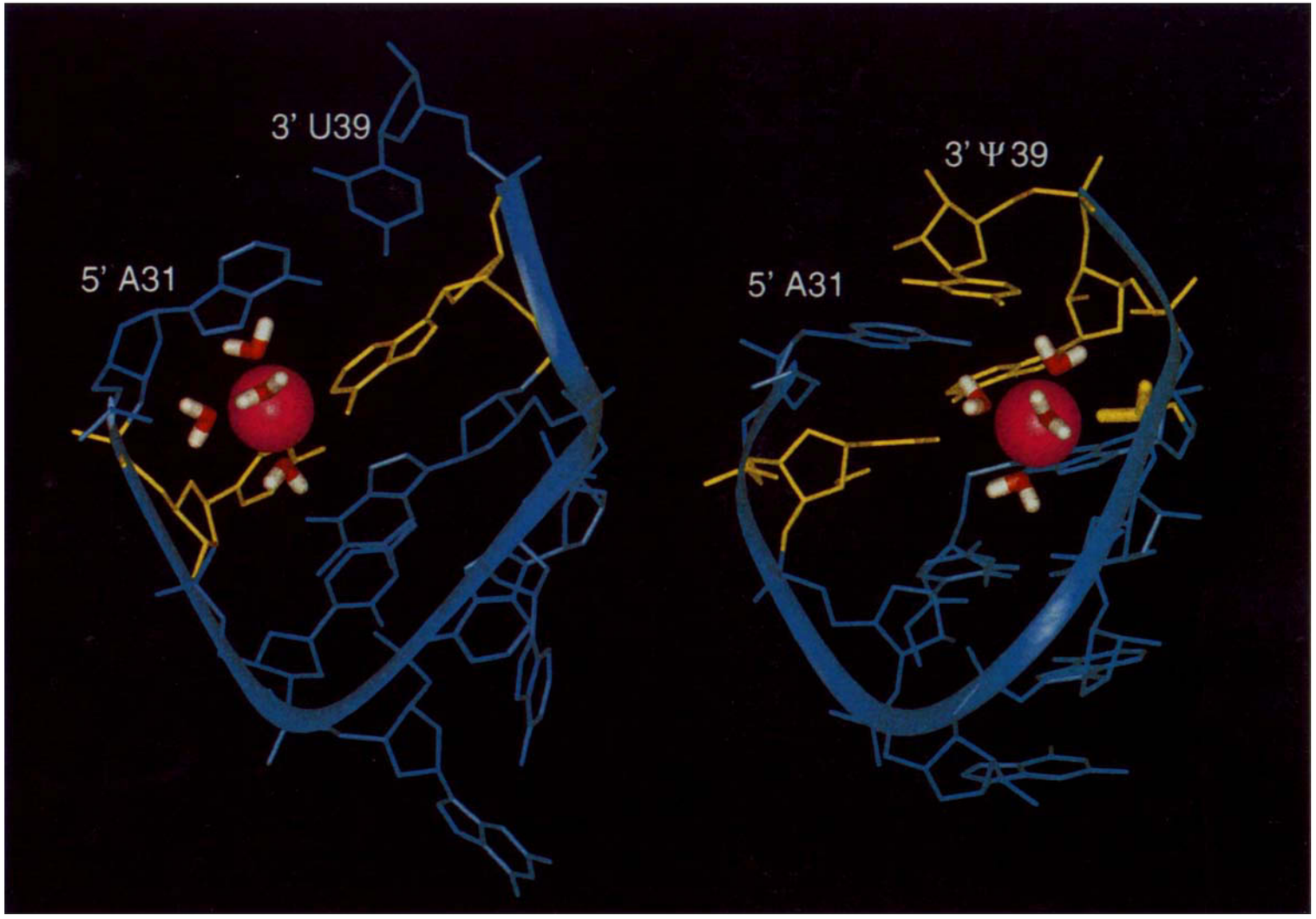

Plate 1. Representation of the Mg^{2+} binding sites of $fDNA^{Phe}_{AC}$ (left) and the anticodon domain of yeast $tRNA^{Phe}$ (right) showing coordinating ligands. In the averaged $tDNA^{Phe}_{AC}$ structure Mg^{2+} is coordinated by four waters and two bases (yellow). Mg^{2+} in the crystal structure of $tRNA^{Phe}$ uses five waters (one hidden) and one phosphate oxygen (thick yellow) to coordinate Mg^{2+}. Secondary ligands of the water molecules in the $tRNA^{Phe}_{AC}$ are in yellow.

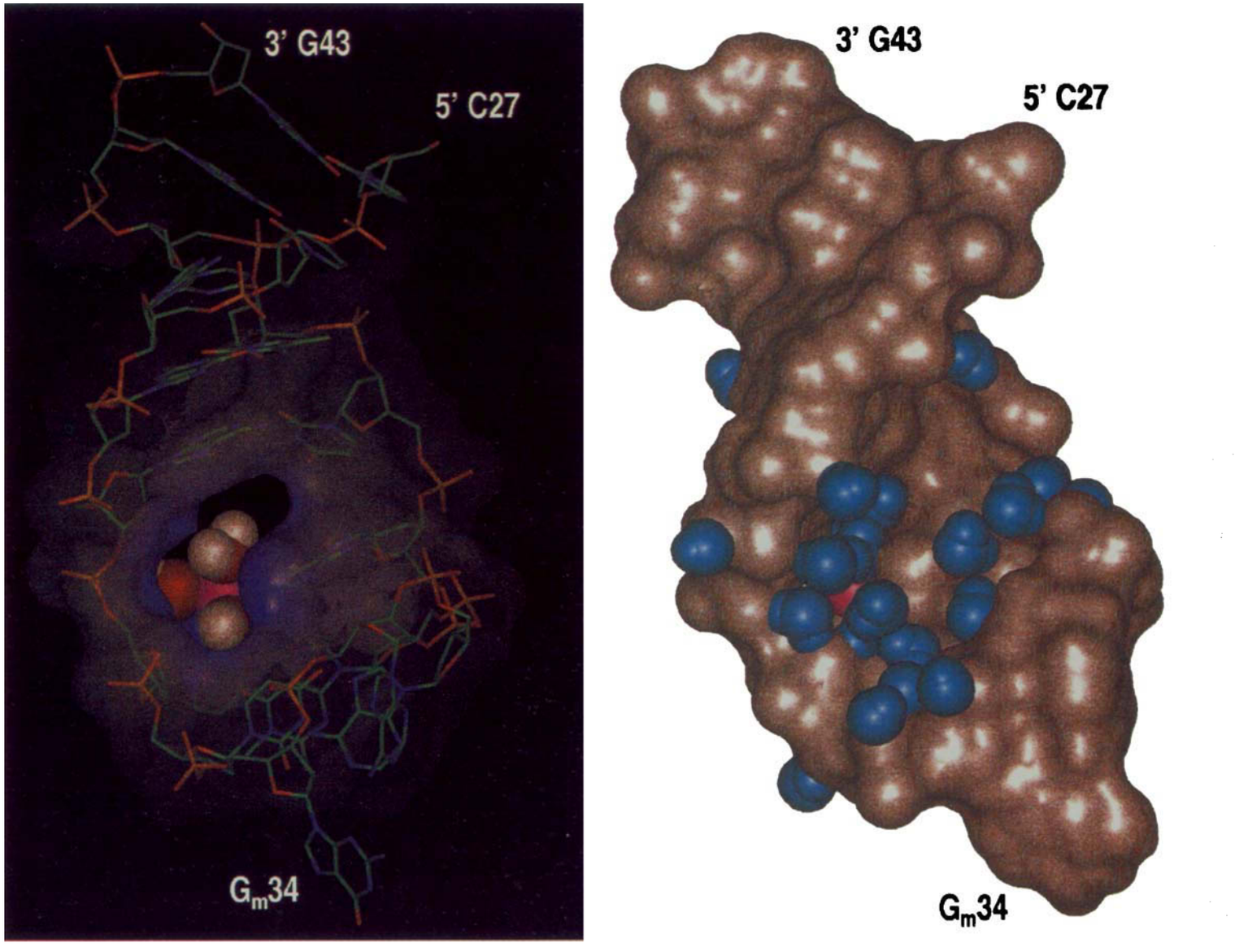

Plate 2. Net electrostatic potential of $tDNA^{Phe}_{AC}$ and surface waters. On the left of the figure, the averaged $tDNA^{Phe}_{AC}$ structure is depicted with a hydrated Mg^{2+} (in violet) and coordinating waters in the binding pocket. The translucent surface of the tDNA molecule is colored according to the electrostatic potential contributions of just Mg^{2+} (5 – 0 *kT*). Thus, the surface around Mg^{2+} is positive (blue/opaque) and further away is neutral (white/transparent). On the right of the figure, the surface of $tDNA^{Phe}_{AC}$ is depicted with stable water molecules surrounding Mg^{2+} (in violet) and between the stem and loop. Na^+ counter ions are not shown.

than did the tDNA analogue[19] and one may suspect that the 2′-OH in tRNA may contribute a ligand. However, in the $tRNA^{Phe}$ crystal structure, Mg^{2+} in the anticodon was not coordinated by hydroxyls. Therefore, the global ribose backbone conformation in $tRNA^{Phe}$ may allow for a better binding site than the deoxyribose in the analogue.

The introduction of a +2 charge to a molecule the size of $tDNA^{Phe}_{AC}$–d(m^1G_{37} ; m^5C_{40}) should affect the molecules overall electrostatic potential, $\phi(r)$, but especially that local to the binding site. To evaluate the influence of Mg^{2+} on electrostatics, $\phi(r)$ was calculated with and without the Mg^{2+} ion present from which the net electrostatic potential was determined (Plate 2, left). As would be expected, a strong net positive charge (blue color in Plate 2) was evident in the binding pocket and spread to the last base pair in the stem. A large negative potential in the cleft between the stem and the loop was not affected. However, the side of the binding pocket opposite this cleft and the entire area of the loop was neutralized (white color in Plate 2) by the binding of Mg^{2+}. Site-specific binding of Mg^{2+} in the anticodon loop could be an important factor in neutralizing charge repulsion that occurs during anticodon–codon interaction.[42] As RNAs fold, presumably divalent ion and polyamines are more effective at neutralizing electrostatic repulsions of the RNA polyanionic backbone than monovalent ions, as observed with the folding of a 23S rRNA fragment in the presence of Mg^{2+}.[43]

The modification d(m^5C_{40}) facilitated a single site Mg^{2+} binding to $tRNA^{Phe}_{AC}$.[20,21] We have hypothesized that increased hydrophibicity produced by methylation and other hydrophobic modifications would tend to order surface water on nucleic acids.[2] In addition, a bound and hydrated Mg^{2+} ion would be expected to increase the ordering of water around the $tDNA^{PHe}_{AC}$ molecule, but particularly near the binding site. Entropic properties of H_2O cannot be directly detected by NMR. However, as a first approximation thermodynamic parameters can be calculated from the thermal denaturation studies of $tDNA^{Phe}_{AC}$–d(m^1G_{37} ; m^5C_{40}) with and without Mg^{2+} bound.[27] With the binding of Mg^{2+}, the overall stability of the molecule as measured by ΔG increased by 0.5 ± 0.1 kcal mol^{-1} (Table 2). The increased stability was attributed to ΔS because of a decrease in this thermodynamic property by 13 kcal mol^{-1} K^{-1} with little change in ΔH. To ascertain if the decreased ΔS could be associated with an ordering of H_2O, MD simulations were performed to locate water molecules held in the tDNA's first solvation shell (Fig. 9, right). The most static H_2O molecules were the four coordinating Mg^{2+}. Outward from the binding pocket into the cleft, an additional 15 (of 1703 remaining) waters remained stationary during most of the MD (Fig. 9, right). Several others waters were found coordinating Na^+ counter ions.

CONCLUSION

NMR signal assignments for non-standard nucleic acid structures are difficult to achieve.[44] However, DNA signal assignments are easier than that of RNAs because of the presence of H2″ and the relatively wider chemical shift dispersion of the deoxyribose *vs.* ribose resonances. Nucleic acids have only four spin systems compared with the 20 different spin systems of proteins. However, sequential signal assignments in nucleic acid double helical stems, via imino base paired proton NOEs, have become routine and limitations due to a lack of unique spin systems are partly overcome by selective ^{15}N and ^{13}C enrichments. Localization of the single Mg^{2+} binding site was readily accomplished by NMR. Because $tRNA^{Phe}_{AC}$–(m^1G_{37} ; m^5C_{40}) and $tDNA^{Phe}_{AC}$–d(m^1G_{37} ; m^5C_{40}) of identical base sequence bind Mg^{2+}, the 2′-OH could not be involved in metal coordination. Individual signal broadening was detected by Mn^{2+} titration of a 1.3 mM tDNA even in the presence of 5 mM Mg^{2+}. Mg^{2+} stabilized and ordered the tDNA loop and neutralized the negative charge in the loop. These changes would be expected to promote interaction of tRNA and its DNA analogue with mRNA codons.[22] Even the simplest of nucleoside modifications, a methylation, significantly altered the chemistry and structure of a nucleic acid. Although the site of Mg^{2+} coordination has been determined, the roles played by the modified nucleosides remains obscure. We propose that methylation of C_{40} in $tRNA^{Phe}$ and in the DNA analogue produced, through changes in base stacking and surface water, a Mg^{2+} binding pocket in the anticodon loop at the end of the anticodon stem. Differences in base stacking could be investigated by comparing the $tDNA^{Phe}_{AC}$–d(m^1G_{37} ; m^5C_{40}) and unmodified $tDNA^{Phe}_{AC}$ structures. However, in the absence of modified nucleosides the dynamics of $tDNA^{Phe}_{AC}$ preclude an NMR study of structure.[20,21] The design and structural determination by NMR of DNA molecules that are biologically active analogues of RNA has numerous advantages.[22] Chemical synthesis and examination of the structure–function relationships of these molecules yields significant insight into the physico-chemical roles of modified nucleosides and their potential use in the design of therapeutic agents.[2]

Acknowledgements

We gratefully acknowledge provision of the protected d(m^1G) phosphoramidite by Dr Adam Kraszewski and colleagues of the Polish Academy of Sciences (Poznan), the assistance of the NCSU Biochemistry/Chemistry NMR Facility and its staff and the encouragement and support of all of our families. This work was supported by the National Institutes of Health (NIGMS) through grant GM23037 to P.F.A.

Table 2. Thermodynamic parameters of $tDNA^{Phe}_{AC}$–d(m^1G_{37} ; m^5C_{40})

	ΔH (kcal mol^{-1})	ΔS (kcal mol^{-1} K^{-1})	$\Delta G_{37\,°C}$ (kcal mol^{-1})	T_m (°C)
No Mg^{2+}	−18 ± 2	−59 ± 7	−0.38 ± 0.11	42.8 ● 0.5
With 10 mM Mg^{2+}	−23 ± 3	−72 ± 9	−0.72 ± 0.10	47.0 ● 0.7

REFERENCES

1. G. R. Bjork, in *Transfer RNA in Protein Synthesis*, edited by D. L. Hatfield, B. J. Lee and R. M. Pirtle, pp. 23–85. CRC Press, Boca Raton, FL (1992).
2. P. F. Agris, *Prog. Nucl. Acids Res. Mol. Biol.* **53**, 79 (1996).
3. P. F. Agris, in *Encyclopedia of NMR*, edited by D. M. Grant and R. K. Harris, pp. 4151–4158. Wiley, Chichester (1996).
4. K. B. Hall, J. R. Sampson, O. C. Uhlenbeck and A. G. Redfield, *Biochemistry* **28**, 5794 (1989).
5. C. S. Chow, L. S. Behlen, O. C. Uhlenbeck and J. K. Barton, *Biochemistry* **31**, 972 (1992).
6. J. R. Sampson, L. S. Behlen, A. B. DiRenzo and O. C. Uhlenbeck, *Biochemistry* **31**, 4161 (1992).
7. G. Striker, D. Labuda and M. C. Vega-Martin, *J. Biomol. Struct. Dyn.* **7**, 235 (1989).
8. D. Yue, A. Kintanar and J. Horowitz, *Biochemistry* **33**, 8905 (1994).
9. P. G. Schmidt, H. Sierzputowska-Gracz and P. F. Agris, *Biochemistry* **26**, 8529 (1987).
10. P. G. Schmidt, T. Playl and P. F. Agris, *Biochemistry* **22**, 1408 (1983).
11. P. F. Agris and P. G. Schmidt, *Nucleic Acids Res.* **8**, 2085 (1980).
12. B. Honig and A. Nicholls, *Science* **268**, 1144 (1995).
13. J. Swiatek, *J. Coord. Chem.* **33**, 191 (1994).
14. S. H. Kim, F. L. Suddath, G. J. Quigley, A. McPherson, J. L. Sussman, A. H. J. Wang, N. C. Seeman and A. Rich, *Science* **185**, 435 (1974).
15. G. J. Quigley, M. M. Teeter and A. Rich, *Proc. Natl. Acad. Sci. USA* **75**, 64 (1978).
16. S. S. Reid and J. A. Cowan, *Biochemistry* **29**, 6025 (1990).
17. V. Dao, R. Guenther, A. Malkiewicz, B. Nawrot, E. Sochacka, A. Kraszewski, K. Everett and P. F. Agris, *Proc. Natl. Acad. Sci. USA*, **91**, 2125 (1994).
18. G. M. Clore, A. M. Gronenborn, E. A. Piper, L. W. McLaughlin, E. Graeser and J. H. van Boom, *Biochem. J.* **221**, 737 (1984).
19. Y. Chen, H. Sierzputowska-Gracz, R. Guenther, K. Everett and P. F. Agris, *Biochemistry* **32**, 10249 (1993).
20. R. H. Guenther, C. C. Hardin, H. Sierzputowska-Gracz and P. F. Agris, *Biochemistry* **31**, 11004 (1992).
21. V. Dao, R. H. Guenther and P. F. Agris, *Biochemistry* **31**, 11012 (1992).
22. M. M. Basti, J. Stuart, A. T. Lam, R. Guenther and P. F. Agris, *Nature Struct. Biol.* **3**, 38 (1996).
23. N. D. Sincha, J. Biernat, J. McManus and H. Koster, *Nucleic Acids Res.* **12**, 4539 (1984).
24. P. F. Agris, A. Malkiewicz, S. Brown, A. Kraszewski, B. Nawrot, E. Sochacka, K. Everett and R. Guenther, *Biochimie* **77**, 125 (1995).
25. C. W. Gehrke, J. A. Desgres, K. O. Gerhardt, P. F. Agris, G. Keith, H. Sierzputowska-Gracz, M. S. Tempesta and K. C. Kuo, in *Chromatography and Modification of Nucleosides*, edited by C. W. Gehrke and K. C. Kuo, pp. 159–223. Elsevier, Amsterdam (1990).
26. C. R. Cantor, C. R. Warshaw and H. Shapiro, *Biopolymers* **9**, 1059 (1970).
27. L. A. Marky and K. J. Breslauer, *Biopolymers* **26**, 1601 (1987).
28. D. G. Davis and A. Bax, *J. Am. Chem. Soc.* **107**, 2820 (1985).
29. G. Wagner and E. R. P. Zuiderweg, *Biochem. Biophys. Res. Commun.* **113**, 854 (1983).
30. J. Williamson and S. G. Boxer, *Biochemistry* **28**, 2819 (1989).
31. A. Kumar, R. R. Ernst and K. Wuthrich, *Biochem. Biophys. Res. Commun.* **95**, 1 (1980).
32. D. J. States, R. A. Haberkorn and D. J. Ruben, *J. Magn. Reson.* **48**, 286 (1982).
33. G. Drobny, A. Pines, A. Sinton, D. P. Weitkamp and D. E. Wemmer, *Fararday Symp. Chem. Soc.* **13**, 49 (1979).
34. S. J. Weiner, P. A. Kollman, D. T. Nguyen and D. A. Case, *J. Comput. Chem.* **7**, 230 (1986).
35. A. Nicholls and B. Honig, *J. Comput. Chem.* **12**, 435 (1991).
36. K. Wüthrich, *NMR of Proteins and Nucleic Acids*. Wiley, New York (1988).
37. J. Lingbeck, M. G. Kubinec, J. Miller, B. R. Reid, G. P. Drobny and M. A. Kennedy, *Biochemistry* **35**, 719 (1996).
38. C. A. G. Haasnoot, H. P. Westerink, G. A. van der Marel and J. H. van Boom, *J. Biomol. Struct. Dyn.* **2**, 345 (1984).
39. W. Bujalowski, E. Greser, L. W. McLaughlin and D. Porschke, *Biochemistry* **25**, 6365 (1986).
40. A. T. Lam, R. Guenther and P. F. Agris, *BioMetals* **8**, 290 (1995).
41. G. Ott, L. Arnold and S. Limmer, *Nucleic Acids Res.* **21**, 5859 (1993).
42. K. A. Sharp, B. Honig and S. C. Harvey, *Biochemistry* **29**, 340 (1990).
43. E. Draper, *Acc. Chem. Res.* **25**, 201 (1992).
44. P. F. Agris and S. C. Brown, *Methods Enzymol.* **261**, 277 (1995).